Role of vitamin C in the protection of the gum and implants in the human body: theoretical and experimental studies

M. Abosaooda,[1] Wajdy J. Majid,[2] E.A. Hussein,[3] A.T. Jalil,[4] M.M. Kadhim,[5,6]* M.M. Abdullah,[3] A.H. Hamed[3] and H.A. Almashhadani[7]

[1]College of pharmacy, The Islamic University, Najaf, 54001, Iraq
[2]Department of Biochemistry, College of Medicine, University of Thi-Qar, Nasiriyah, Iraq
[3]Chemistry Department, University of Baghdad, College of Science for Women, Iraq
[4]Faculty of Biology and Ecology, Yanka Kupala State University of Grodna, Grodna, Belarus
[5]Department of Dentistry, Kut University College, Kut, Wasit, 52001, Iraq
[6]College of Medical Technology, Islamic University, Najaf, Kufa Street, 54001, Iraq
[7]Dentistry Department, Al-Rasheed University College, Iraq
**E-mail: Mustafa_kut88@yahoo.com*

Abstract

The article describes a study on the role of vitamin C as a protective agent for the teeth, gum, and implants using quantum chemical calculations and polarization tests. The Density Functional Theory (DFT) at 6-311G (d, p) basis set is used to estimate the ability of vitamin C to inhibit the corrosion of the abovementioned parts. The experimental study was performed in a at human body media simulator (Hank's balanced salt solution) at a temperature of 37°C. The compound was optimized for its ground state, physical properties, and corrosion parameters. Further, HOMO, LUMO, energy gap, dipole moment, and other parameters were used to predict the inhibitor's efficiency. Gaussian 09, UCA-FUKUI, MGL tools, DSV, and LigPlus software was used. According to electron density, Electrostatic Surface (ESP), Total Electron Density (TED), FUKUI function, and dual descriptor were used to show the active sites of adsorption. Also, docking studies were applied to predict the effect of vitamin C on *A. ferrooxidans* bacteria, which causes eroding the implants. The Ti6Al4V alloy was tested at three concentrations of the VC inhibitor using the polarization method. A concentration of 55 mg/L is the best in terms of inhibitor efficiency (99.62%).

Received: August 21, 2021. Published: September 2, 2021 doi: 10.17675/2305-6894-2021-10-3-22

Keywords: *vitamin C, implants, Hank's balanced solution, docking, FUKUI, dual descriptor.*

1. Introduction

Diverse diseases have shortened mankind's efficiency and lifespan in recent decades. Replacement or implantation of damaged tissues, blood vessels, organs, bones, *etc*. can accelerate this decline. Increasingly complex implantation procedures and materials have reduced surgical risks. Sadly, homogeneous or traditional autogenous prosthetic elements are still scarce [1–3].

Due to restricted material choices, new synthetic implant materials must be developed. These materials should be easier to apply and function well in the body, especially when in touch with bodily fluids. The human body may comprise polymers, ceramics, composites, and metallic implants [4].

Metallic implants may replace skeleton elements [5]. Some of the purposes they were utilized for were bone plates and artificial joints as well as dental implants and spinal fixations. Metallic materials have higher fatigue, tensile, and fracture toughness than other materials (polymers and ceramics). Metallic biomaterials such as 316L stainless steel are frequently utilized. It is very resistant to corrosion and releases little toxins when exposed to bodily fluids [6–8].

Nevertheless, the human body is hard on metals and alloys. So most implanted metallic materials may react chemically or electrochemically. Each of these ions has a specific function in the body. Stainless steel 316L of surgical grade is utilized in many nations. It corrodes in the body, releasing iron and other metallic ions, known irritants and toxins [10]. Implants of stainless steel fail because of pitting and crevice corrosion [11–13].

Human metal corrosion research is vital. Humans using implant materials may utilize vitamins, especially Vitamin C, for a long period. There is little study on Vitamin C's impact on implant materials. The present study investigated the potential effect of vitamin C as a corrosion inhibitor for implants in the human body and provided experimental proof.

2. Calculation Models

To conduct quantum chemical calculations at 37°C, Gaussian 09 software was used to perform density functional theory (DFT) calculations using a hybrid Becke three-parameter Lee, Yang, and Parr function (B3LYP). For the VC structure, we chose the 6-311G (d,p) basis set since it provides precise electrical characteristics and geometries (Figure 1). Fukui function and Dual descriptor were also calculated and discussed using Gaussian 09 and UCA-FUKUI programs. Further, docking calculations and Molecular Graphics Laboratory (MGL) program were used to simulate protein-ligand interactions and other biomolecular systems. All the above-mentioned calculations were used to predict the effect of the inhibitor molecule on inhibition of corrosion due to *A. ferrooxidans* bacteria [14]. The protein structure of *A. ferrooxidans* (3f9s) was downloaded from the Research Collaboratory for Structural Bioinformatics (RCSB) [15]. The protein and inhibitor structures were tested using the ADT tool in the Molecular Graphics Laboratory program [16]. Using DSV software to identify the molecule's root, the Autodock was performed automatically [17].

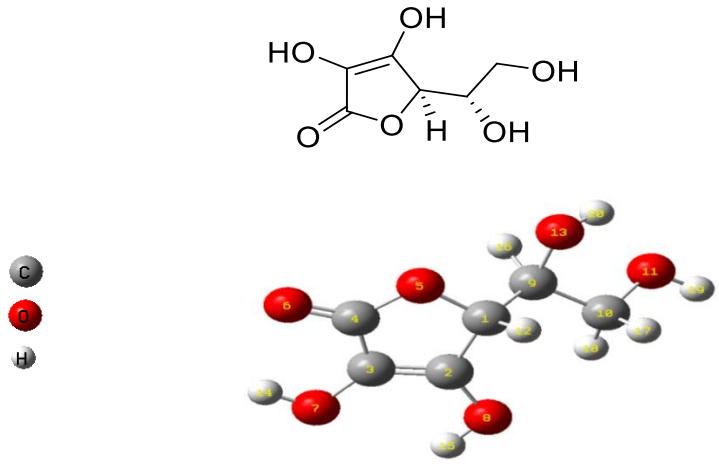

Figure 1. The geometry of the inhibitor (VC) in the ground state, calculated at equilibrium using DFT (B3LYP/6-311+G (d, p)) methods.

3. Results and Discussion

3.1. Inhibition parameters

In this study, the 6-311G (d,p) basis set was utilized, which provides precise electrical characteristics, geometries, and statistics (Figure 1) [18]. The calculations were performed in a vacuum at 37°C [19, 20]. Limit orbital theory was used to predict the interaction of the inhibitor molecule with the surface of the metal [21]. It involves the frontier molecular orbital (FMO) which gives very significant evidence for the stability by means of the difference in energy of the frontier orbitals as $\Delta E = E_{LUMO} - E_{HOMO}$.

Inhibitors with high E_{HOMO} values have a propensity to donate electrons. When it comes to the LUMO energy (E_{LUMO}), the lower the value, the greater the molecule's propensity to accept electrons. Chemical quantum parameters are related to the inhibition efficiency of the molecule, such as the energies of highest occupied and lowest unoccupied molecular orbitals (E_{HOMO} and E_{LUMO}), the energy gap ($\Delta E = E_{LUMO} - E_{HOMO}$), electronegativity ($\chi$), dipole moment ($\mu$), ionization potential (*IP*), electron affinity (*EA*), and the global softness (*S*) as shown in Table 1. When the energy gap (ΔE) of the border orbitals reduces, the inhibitor's efficiency increases [22]. According to Koopman's hypothesis, the ionization potential (*IP*) and electron affinity (*EA*) are related to the negative of both HOMO and LUMO energy, respectively [23]:

$$IP = -E_{HOMO} \quad (1)$$

The energy needed to remove an electron from an atom is denoted by *IP*. A low value of ionization energy refers to high inhibition efficiency.

$$EA = -E_{LUMO} \quad (2)$$

Electron affinity (*EA*) is defined as the released energy when an electron is introduced to a neutral atom. The higher the value of electron affinity, the less stable the system and the greater the inhibition efficiency. Hardness (η) is defined as the second derivative of *E*, which predicts both stability and reactivity of the molecule [24].

$$\eta = \frac{IP - EA}{2} \tag{3}$$

$$\chi = \frac{IP + EA}{2} \tag{4}$$

Electronegativity (χ) is an atom's capacity to remove shared electrons to its side. Low electronegativity value refers to high inhibition efficiency.

The inverse of the global hardness (*H*) is the global softness (*S*) [25]. It is a critical characteristic for determining the stability and reactivity of molecules:

$$S = \frac{1}{\eta} \tag{5}$$

The global electrophilicity index (ω) developed by Parr [26, 27] is a measure of a molecule's stabilization energy after accepting extra electrons. The low value of this index refers to good inhibitors.

$$\omega = \frac{(-X)^2}{2\eta} \tag{6}$$

The results presented in Table 1 refer to the ability of VC to inhibit the corrosion that implants undergo. The optimized geometries of the investigated molecule in the gas phase, including the LUMO and HOMO density distributions, are shown in Figure 2. The red color refers to high electron density sites, while the green color shows low electron density ones [28]. High electron density is a region that donates electrons to the metal surface, while green is an area that accepts electrons from the metal surface [29]. As a result, the distribution of these two regions is critical. VC has high electron density on the acceptor site, which is caused by the conjugation in the C=C–C=O structure. Oxygen atoms in OH groups represent the donating region.

Table 1. The results of DFT calculation of a number of physical characteristics of the inhibitor molecule in vacuum at equilibrium geometry for the ground and protonated states.

Comp.	E_{HOMO} **(eV)**	E_{LUMO} **(eV)**	$\Delta E_{HOMO-LUMO}$ **(eV)**	**μ (Debye)**
VC	–6.60544088	–0.979632	5.625809	5.6059
ω (eV)	***S* (eV)**	**η (eV)**	**χ (eV)**	***EA* (eV)**	***IE* (eV)**
2.556669	0.355504	2.812904	3.792536	0.979632	6.605441

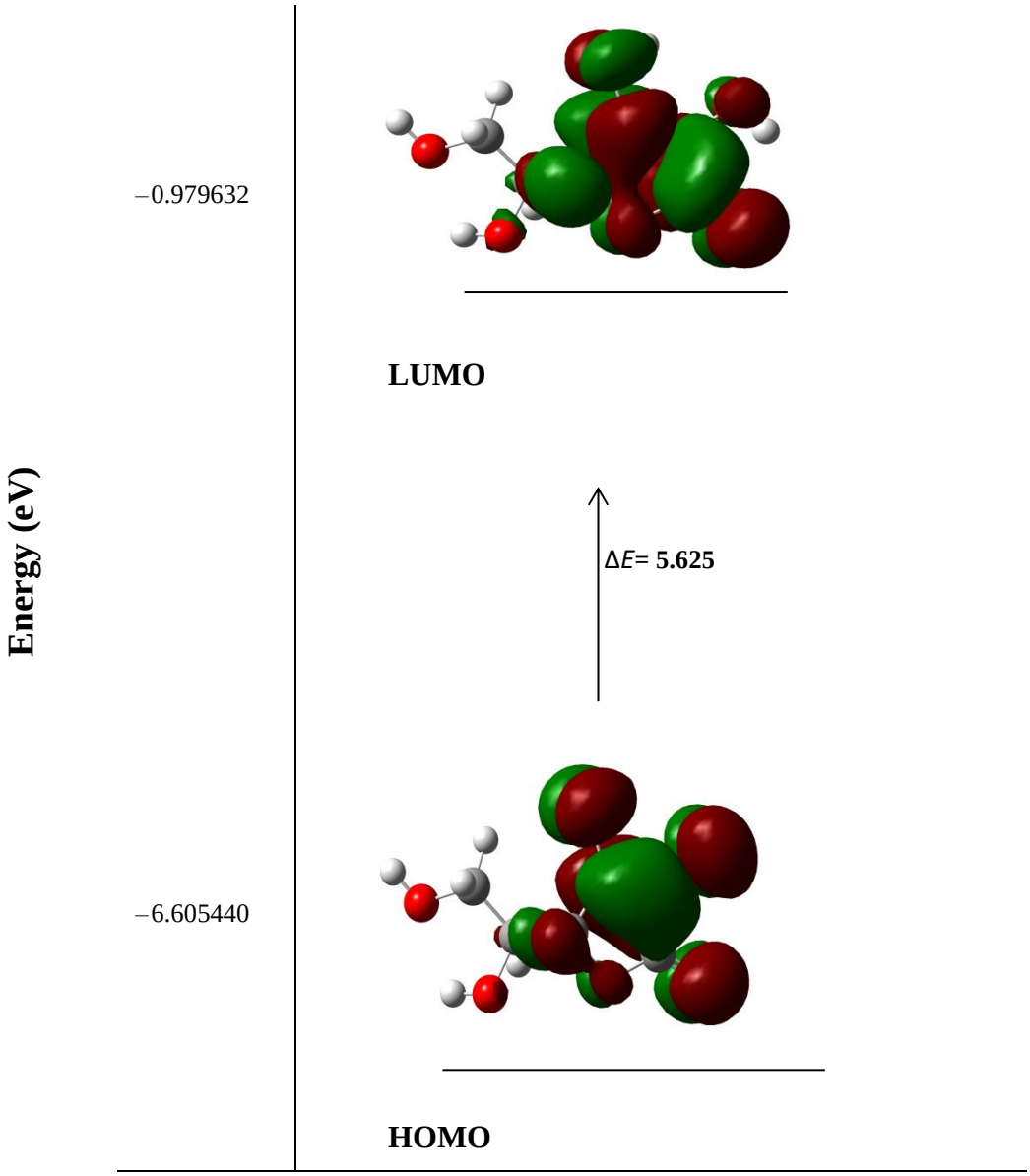

Figure 2. HOMO and LUMO orbital energy levels in the ground state.

3.2. Electron density maps

The strength of adsorption can be predicted based on the electron density of the donor atom. The total electron density (TED) represents the molecule's electron density. The red color in Figure 3 refers to the high electronegativity sites, such as the O atoms of (OH) and carbonyl groups in investigated compounds, which may aid in electrophilic attack. Furthermore, atoms having a moderate electronegativity are represented by yellow color. The blue region refers to the most favorable positive area, which accepts electrons from donor atoms [30]. The electrostatic surface potential (ESP) depicts the adsorption orientation of the molecule

on the metal surface (Figure 3), which is in same orientation with the carbonyl and hydroxyl groups [31].

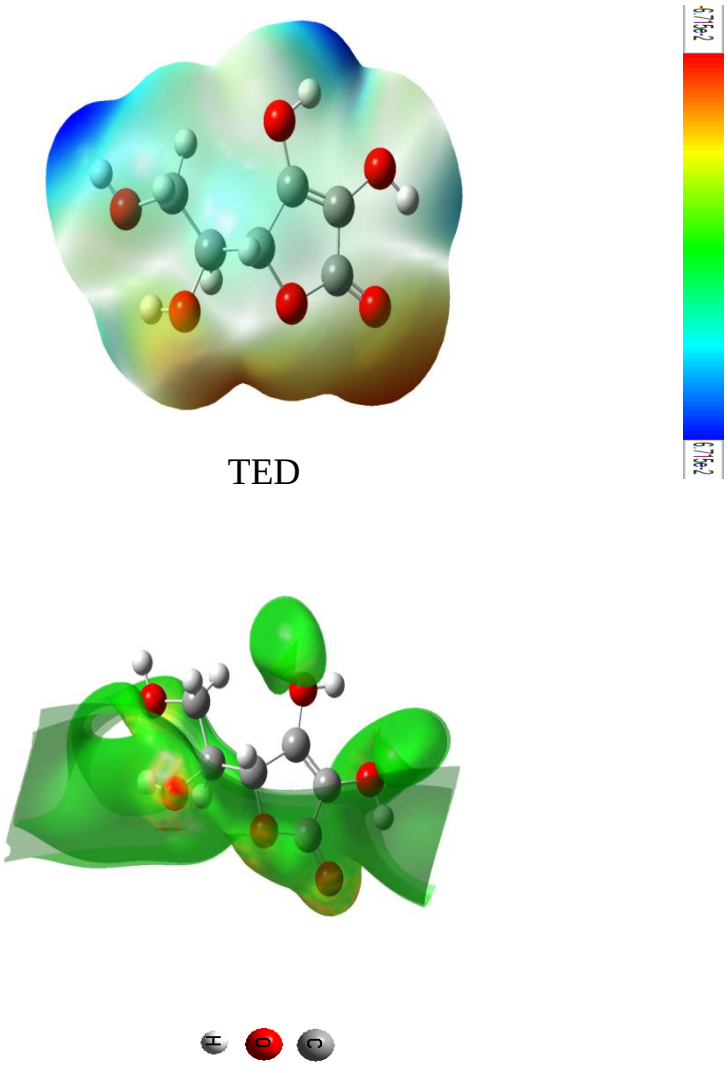

Figure 3. TED, ESP maps of VC at the 6-311G (d,p) basis set.

3.3. Fukui function

The Fukui function (f_x) is defined as the derivative of the electron density in terms of the number of electrons N at a constant external potential. It permits the identification of the most active locations within the optimized structures' functional groupings. The Fukui functions [18, 32] dependent on the direction of electron transport were estimated using finite difference approximations obtained from population analysis of atoms in molecules or compounds. To show the location that accepts or donates electrons, the dual descriptor is essential [33].

Fukui and Dual function were calculated using the DFT method at (6-311G/d, p) basis set with Gaussian 09 and USA FUKUI software. The inhibitor's three-dimensional structure with atom numbering is showing in Figure 1. The (f_+) of the atom represents the ability to accept an electron, and (f_-) represents the ability to donate an electron, while (f) is the state of the free radical Table 2. According to Dual Descriptor, the electrophilic atoms are C1, C2, C4, O5, H12, H15, H17, and H19, while the nucleophilic ones are C3, O6, O7, O8, O9, O11, O13, H14, H16, and H18. Fukui function presents the more active atoms (Figure 4) in the electrophilic state (C2, C4) and nucleophilic state (C2, C3, O6, O7, O8) as shown in Table 2.

Table 2. The inhibitor atoms in f_+, f_-, and f states, and Dual descriptor.

Atoms	f_+	f_-	f	Dual Descriptor
C1	0.0129	0.0120	0.0125	0.0009
C2	0.2469	0.1700	0.2084	0.0770
C3	0.0730	0.1881	0.1306	–0.1150
C4	0.1231	0.0051	0.0641	0.1180
O5	0.0282	0.0124	0.0203	0.0158
O6	0.1019	0.1053	0.1036	–0.0034
O7	0.0161	0.2066	0.1113	–0.1905
O8	0.0509	0.1696	0.1102	–0.1186
C9	0.0270	0.0580	0.0425	–0.0310
C10	0.0037	0.0004	0.0021	0.0033
O11	0.0005	0.0012	0.0009	–0.0007
H12	0.0566	0.0260	0.0413	0.0306
O13	0.0030	0.0038	0.0034	–0.0008
H14	0.0000	0.0003	0.0001	-0.0002
H15	0.0008	0.0002	0.0005	0.0006
H16	0.0002	0.0010	0.0006	–0.0009
H17	0.0055	0.0000	0.0027	0.0054
H18	0.0001	0.0002	0.0002	–0.0001
H19	0.0005	0.0000	0.0002	0.0004

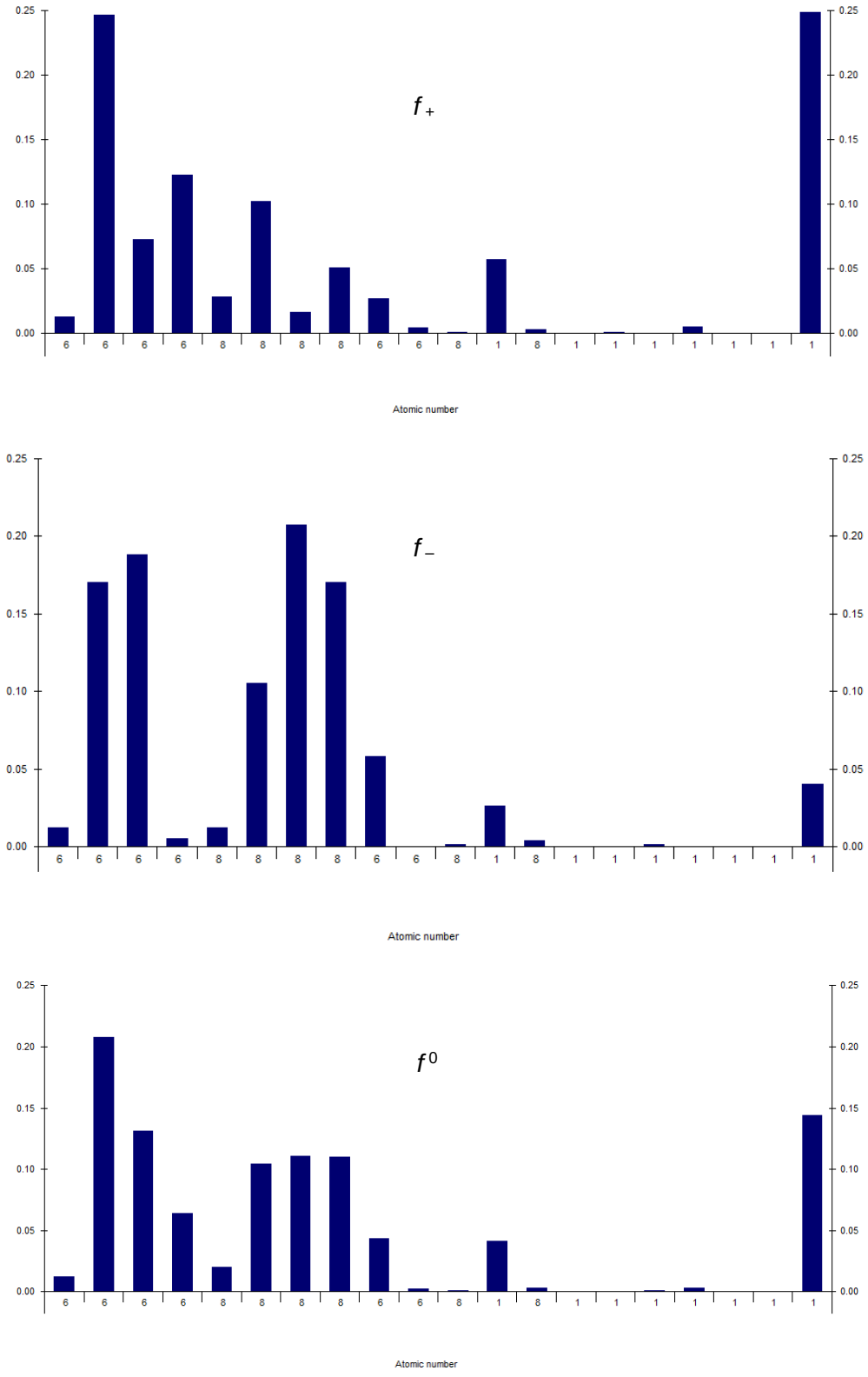

Figure 4. Ground state Fukui functions of the inhibitor.

3.4. Docking studies

To create a stable complex, docking studies could predict the preferred orientation of a molecule with respect to another. The degree of binding between two molecules may be predicted using information about preferred orientation. *Acidithiobacillus ferrooxidans* has been implicated in bacterial corrosion, and the VC compound was examined as a possible inhibitor of *A. ferrooxidans*. Because hydrogen is a receptor for electrons, *Acidithiobacillus ferrooxidans* bacteria induce corrosion.

The binding energy E_b assesses the affinity of the chemical to the receptor protein, whereas the binding efficiency *LE* describes the capacity of the ligand to reach the receptor protein [35]. According to its E_b value (–2.5 kcal/mol), VC has high probability to inhibit *A. ferrooxidans* bacteria (Table 3). It has different sites on the receptor, and the favorite one was number 10 (Figure 5). In addition, DSV and LigPlus simulations revealed the active site and linkage with amino acids of *A. ferrooxidans* structure (Figure 5). Vitamin C showed four hydrogen bonds with amino acids, two of them with serine (SER) and one with each of leucine (LEU) and lysine (LYS). The bond length $O_{(VC)}$–$NH_{(SER)}$ is 3.01 Å, $O_{(VC)}$–$HO_{(SER)}$ is 2.91 Å, $O_{(VC)}$–$NH_{(LEU)}$ is 3.12 Å, and $O_{(VC)}$–$NH_{(LYS)}$ is 2.62 Å (Figure 6) [36].

Table 3. Inhibitor's binding energy and ligand efficiency.

Compound	E_b (kcal/mol)	*LE*	E_b range	Best site number
VC	–2.5	–0.21	–1.18 to –2.5	10

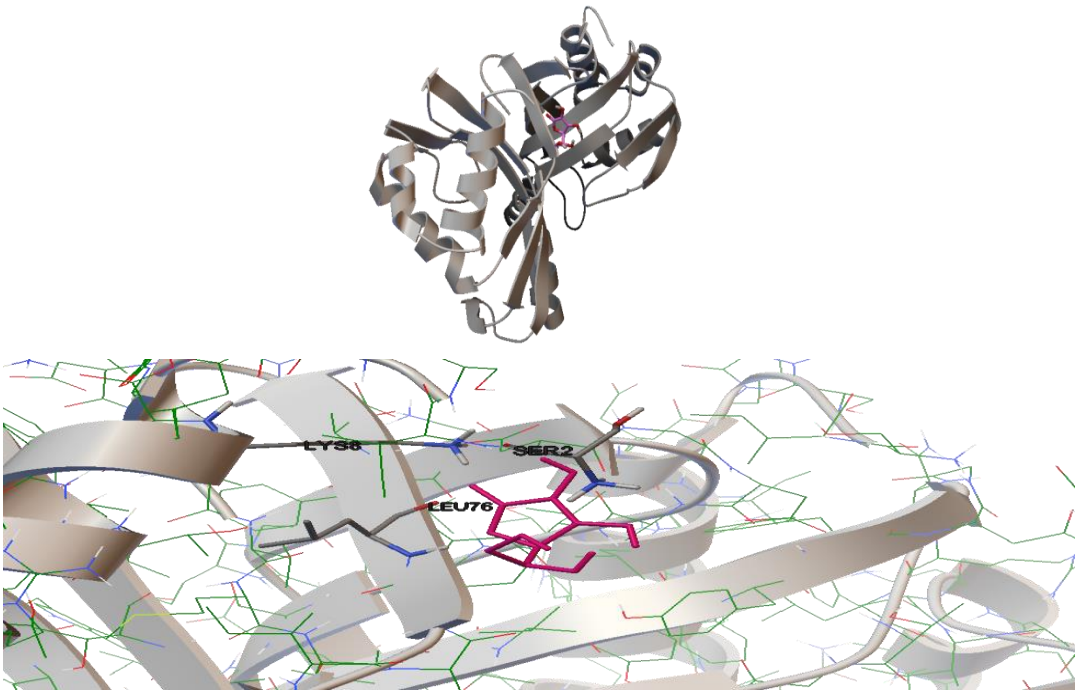

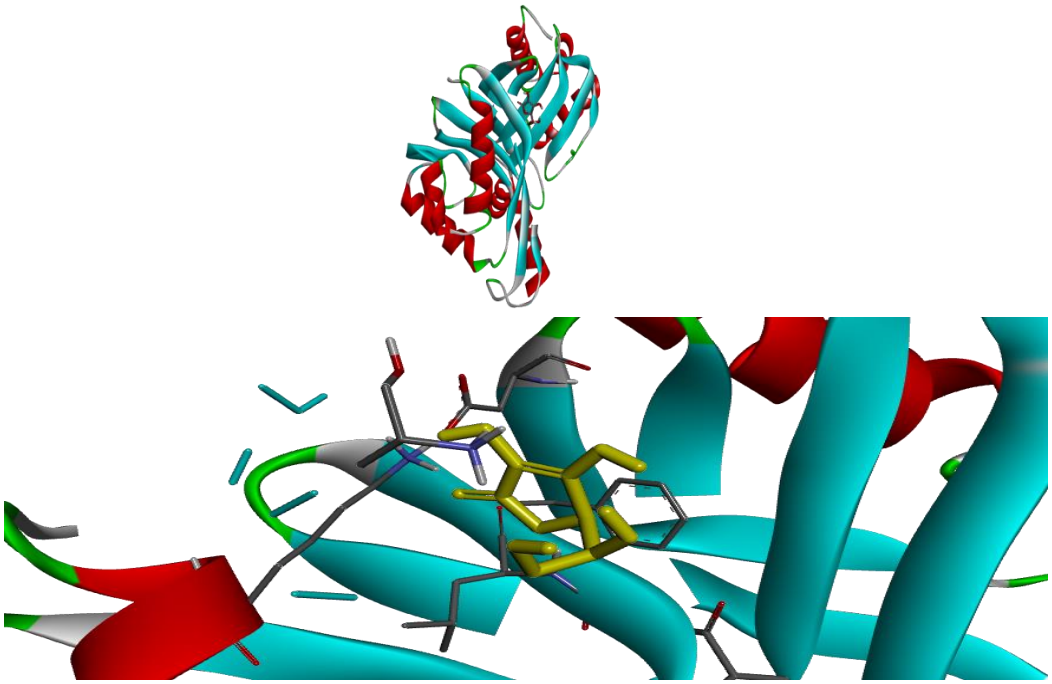

Figure 5. Vitamin C with AF protein bacteria by (MGL tool and DSV software).

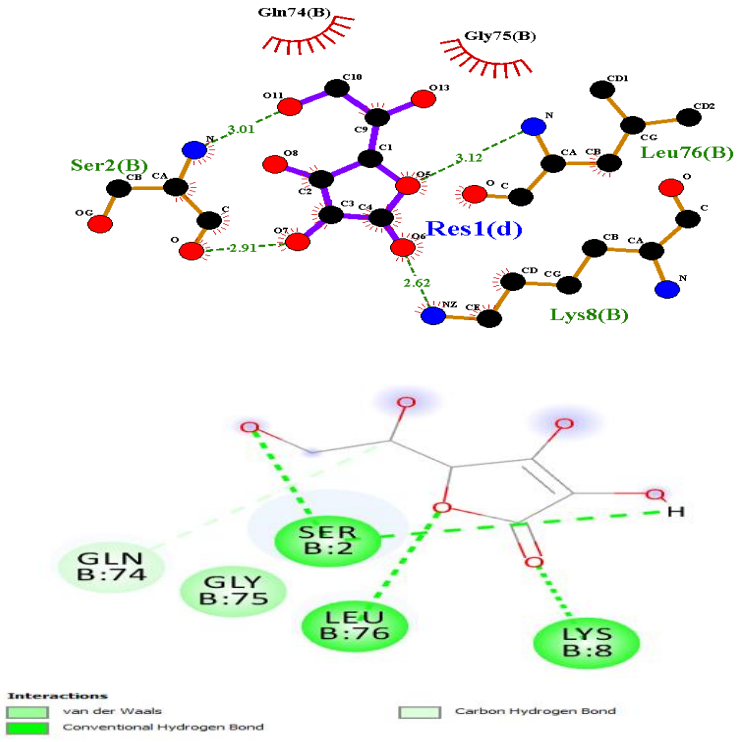

Figure 6. 2D interactions of VC with AF bacteria amino acids.

4. Experimental

4.1. Corrosion Test

Hank's balanced salt solution was used to measure the corrosion behavior of Ti6Al4V samples (HBSS). Table 4 presents the composition of Hank's solution, which has pH 7.4 at 37±1°C [37]. Working electrodes were made from as received Ti6Al4V samples with an exposed area of 1 cm. SCE and platinum were the reference and counter electrodes, respectively. Electrodes were placed into a 1 L corrosion cell with Hank's solution at 37°C. After an initial delay of 900 sec at open circuit conditions, the Ti6Al4V samples were polarized in anodic direction.

Table 4. The composition of Hank's solution.

Component	Amount per liter	Concentration
NaCl (mw: 58.44 g/mol)	8 g	0.14 M
KCl (mw: 74.55 g/mol)	400 mg	0.005 M
$CaCl_2$ (mw: 110.98 g/mol)	140 mg	0.001 M
$MgSO_4–7H_2O$ (mw: 246.47 g/mol)	100 mg	0.0004 M
$MgCl_2–6H_2O$ (mw: 203.303 g/mol)	100 mg	0.0005 M
$Na_2HPO_4–2H_2O$ (mw: 177.99 g/mol)	60 mg	0.0003 M
KH_2PO_4 (mw: 136.086 g/mol)	60 mg	0.0004 M
D-Glucose (Dextrose) (mw: 180.156 g/mol)	1 g	0.006 M
$NaHCO_3$ (mw: 84.01 g/mol)	350 mg	0.004 M

4.2. Polarization Results

The corrosion parameters at 310 K (37°C) obtained from the polarization curves were calculated, recorded and listed in Table 5. None of the values of either b_a or b_c differed significantly. In this experiment, it was shown that ascorbic acid acted as both anodic and cathodic inhibitor. This indicates that adsorption of the inhibitor on a Ti6Al4V surface impeded the metal-to-corrosive medium interaction, leading to reduced i_{corr} values [38].

The percentage inhibition efficiency from Tafel polarization (%*IE*) is listed in Table 5. These values were calculated using the following equation [39, 40]:

$$\%IE = \frac{i_{corr}^0 - i_{corr}}{i_{corr}^0} \times 100 \quad (7)$$

Where i_{corr}^0 and i_{corr} are the corrosion rates without and in the presence of ascorbic acid, respectively. Ascorbic acid was an excellent inhibitor for Ti6Al4V in Hank's Balanced Salt Solution (HBSS).

As one can see in Figure 7, the inhibitory efficiency of ascorbic acid does not have a direct correlation with its concentration and has a maximum at a concentration of 55 mg/L. The primary cause of this is that ascorbic acid is adsorbed onto the titanium surface and produces a barrier that blocks the development of a reaction environment on the titanium surface. Under the influence of ascorbic acid, the corrosion potential changed negatively, though the inhibitor concentration did not change. It is therefore evident that ascorbic acid is an effective inhibitor of corrosion of Ti6Al4V in Hank's solution that affects both anodic and cathodic reactions [41].

Table 5. Corrosion kinetic parameters for Ti6Al4V alloys in Hank's solution at 310 K without and with different concentration of ascorbic acid.

Conc. mg/L	E_{corr}/ mV	i_{corr}/μA·cm^{-2}	b_c/mV·dec^{-1}	b_a/mV·dec^{-1}	R_p/kΩ·cm^2	%*IE*
0	–515.9	3.800	158.0	400.2	12.94394	–
45	–862.5	0.0292	218.9	337.5	4003.833	99.23
55	–896.9	0.0144	294.2	430.0	2597.621	99.62
65	–980.7	0.0232	204.0	321.1	2334.783	99.39

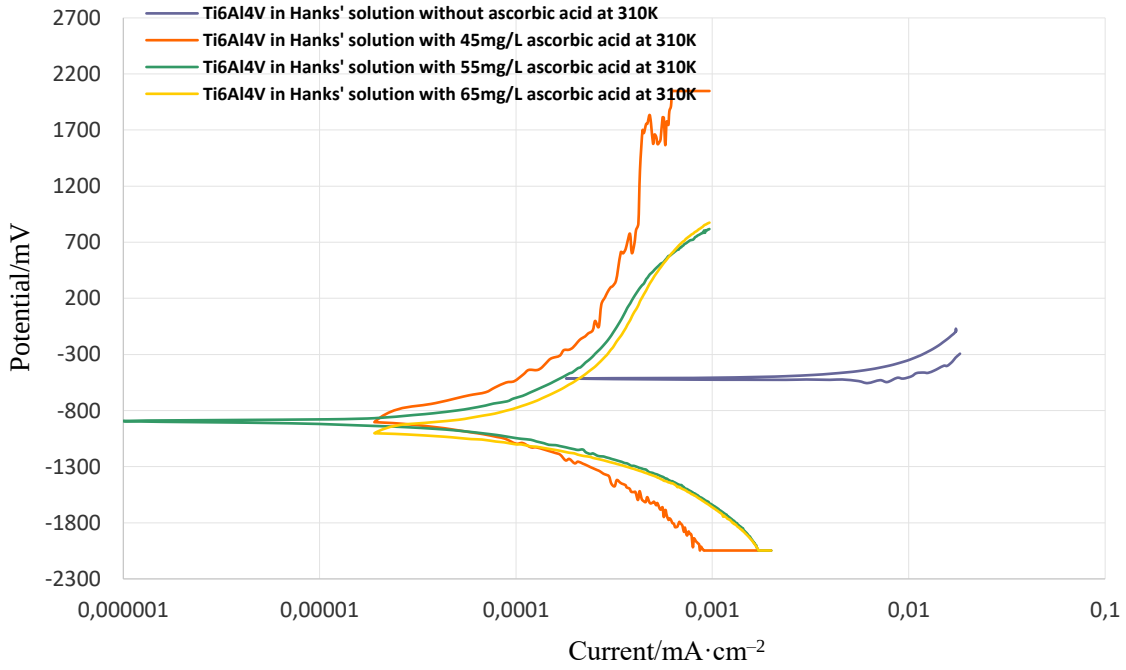

Figure 7. Polarization plots of Ti6Al4V alloy in Hank's solution at 310 K without and with different concentrations of ascorbic acid.

The SEM micrographs of Ti6Al4V after corrosion tests without and with 55 mg/L ascorbic acid are shown in Figure 8. Figure 8a shows the surface of titanium after conducting

the corrosion test. While no ascorbic acid was present, the corrosion of titanium increased because of the titanium's rapid dissolution rate. However, the coating was shown to be durable after conducting the corrosion test in Hank's solution in the presence of ascorbic acid [42]. Dehydration of the surface, which occurs before the SEM photography, causes fractures to appear in the film. A test that verifies the presence of ascorbic acid in a solution on a titanium surface indicates that ascorbic acid has been absorbed by the titanium surface and insulated the surface from the extracellular fluid based on Hank's solution.

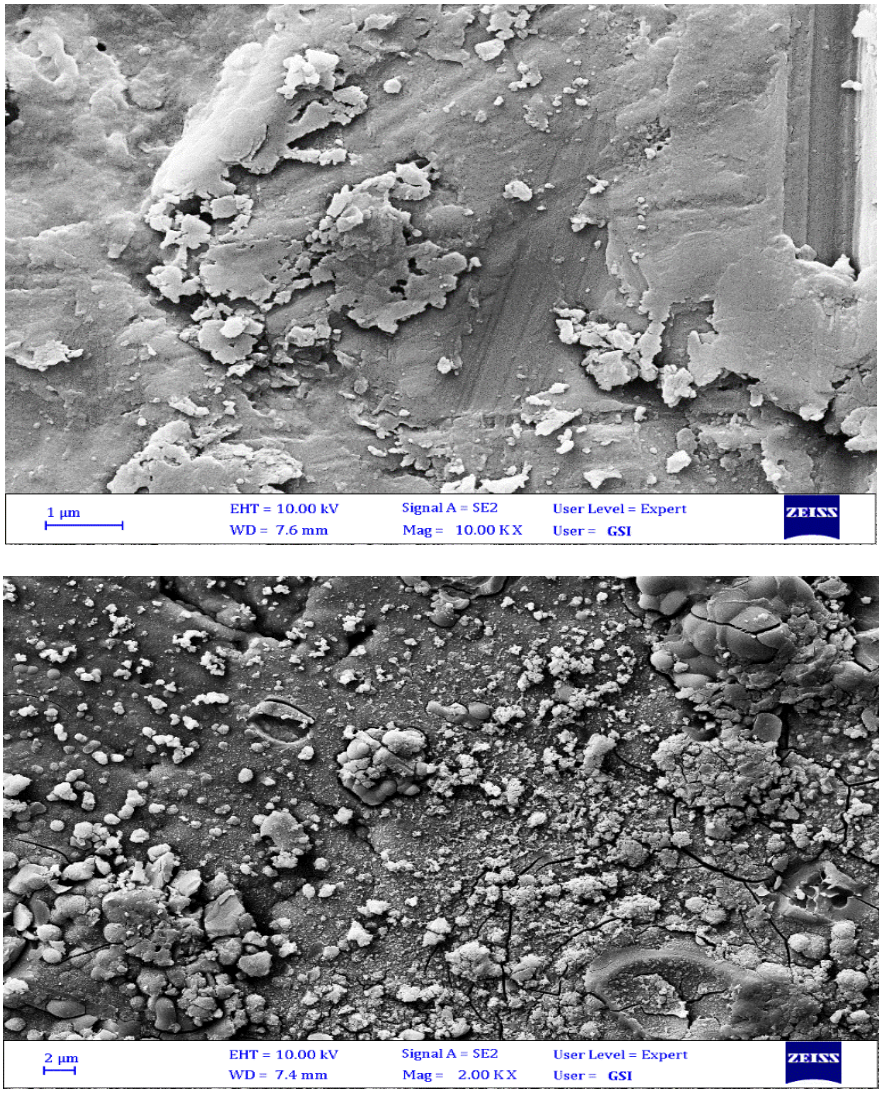

Figure 8. Scanning electron micrographs of Ti6Al4V surface after corrosion tests: a) without ascorbic acid and b) with 55 mg/L ascorbic acid.

5. Conclusions

To investigate the activity of VC as a corrosion inhibitor in its ground state at 37°C, quantum mechanical calculations and DFT were employed. Tafel polarization curves were recorded in Hank's solution with Ti6Al4V used in implants. According to the tested parameters and

adsorption characteristics, the results show that favorable suppression of corrosion occurs. Docking study refers to the ability of VC to reduce the activity of *A. ferrooxidans* bacteria, depending on E_b (–2.5 kcal/mol)) and *LE* (–0.21) values. The experimental part proved the theoretical investigation. The inhibitor efficiency (%*IE*) of the studied concentrations (45, 55 and 65 mg/L) amounts to 99.23, 99.62 and 99.39%.

References

1. N. Eliaz, Corrosion of Metallic Biomaterials: A Review, *Materials*, 2019, **12**, no. 3, 407. doi: 10.3390/ma12030407
2. T. Hanawa, In vivo metallic biomaterials and surface modification, *Mater. Sci. Eng*., 1999, **267**, 260–266.
3. S. Zhang, *Hydroxyapatite Coatings for Biomedical Applications*, CRC Press, Boca Raton, FL, USA, 2013.
4. O. Dincel, I. Simsek and D. Özyürek, Investigation of the wear behavior in simulated body fluid of 316L stainless steels produced by mechanical alloying method, *Eng. Sci. Technol. Int. J*., 2021, **24**, 35–40.
5. U. Kamachi Mudali, T.M. Sridhar and Baldev RAJ, Corrosion of bio implants, *Sadhana*, 2003, **28**, pp. 601–637. doi: 10.1007/BF02706450
6. M. Sivakumar and S. Rajeswari, Investigations of failures in stainless steel orthopaedic implant devices: Pit induced stress corrosion cracking, *J. Mater. Sci. Lett*., 1992, **11**, no. 15, 1039–1042. doi: 10.1007/BF00729754
7. B. Priyadarshini, M. Rama, Chetan and U. Vijayalakshmi, Bioactive coating as a surface modification technique for biocompatible metallic implants: A review, *J. Asian Ceram. Soc*., 2019, **7**, 397–406.
8. J. Jiang, G. Han, X. Zheng, G. Chen and P. Zhu, Characterization and biocompatibility study of hydroxyapatite coating on the surface of titanium alloy, *Surf. Coat. Technol*., 2019, **375**, 645–651.
9. C. Monika, K. Engvall, J. Pan and A. Kotarba, Silane–parylene coating for improving corrosion resistance of stainless steel 316L implant material, *Corros. Sci*., 2011, **53**, 296–301.
10. A.M. Magheru, B. Ghiban, N. Ghiban and I. Antoniac, Corrosion Behaviour in Ringer Solution of Ti-Mo Alloys used for Orthopaedic Biomedical Applications, *Solid State Phenom*., 2012, **188**, 98-101. doi: 10.4028/www.scientific.net/SSP.188.98
11. F. Silver and C. Doillon, *Biocompatibility: Interactions of biological and implantable materials*, 1989, New York, VCH Publishers, vol. 1.
12. D. Arcos and M. Vallet-Regí, Substituted hydroxyapatite coatings of bone implants, *J. Mater. Chem. B*, 2020, **8**, no. 9, 1781–1800. doi: 10.1039/C9TB02710F
13. M. Niinomi, Recent metallic materials for biomedical applications, *Metall. Mater. Trans. A*, 2002, **33**, 477. doi: 10.1007/s11661-002-0109-2

14. B.S. Maluckov, The catalytic role of Acidithiobacillus ferrooxidans for metals extraction from mining - metallurgical resource, *Biodiversity Int. J*., 2017, **1**, no. 3, 109–119. doi: 10.15406/bij.2017.01.00017
15. A. Allouche, Software News and Updates Gabedit – A Graphical User Interface for Computational Chemistry Softwares, *J. Comput. Chem*., 2012, **32**, 174–182.
16. H.M. Berman, J. Westbrook, Z. Feng, G. Gilliland, T.N. Bhat, H. Weissig, I.N. Shindyalov and P.E. Bourne, The Protein Data Bank/Biopython, *Nucleic Acids Res*., 2000, **28**, no. 1, 235–242. doi: 10.1093/nar/28.1.235
17. R.M. Kubba and M.M. Khathem, Theoretical studies of corrosion inhibition efficiency of two new N-phenyl-ethylidene-5-bromo isatin derivatives, *Iraqi J. Sci*., 2016, **57**, no. 2B, 1041–1051.
18. M.M. Kadhim and R.M. Kubba, Theoretical Investigation on Reaction Pathway, Biological Activity, Toxicity and NLO Properties of Diclofenac Drug and Its Ionic Carriers, *Iraqi J. Sci*., 2020, **61**, no. 5, 936–951. doi: 10.24996/ijs.2020.61.5.1
19. A.W. Salman, R.A. Haque, M.M. Kadhim, F.P. Malan and P. Ramasami, Novel triazine-functionalized tetra-imidazolium hexafluorophosphate salt: Synthesis, crystal structure and DFT study, *J. Mol. Struct*., 2019, **1198**, 126902.
20. E.A. Yaqo, R.A. Anaee, H. Abdulmajeed, I. Hameed, R. Tomi and M.M. Kadhim, Electrochemical, morphological and theoretical studies of an oxadiazole derivative as an anti-corrosive agent for kerosene reservoirs in Iraqi refineries, *Mol. Liq*., 2020, **74**, 1739–1757.
21. R.S. Hatam, S.I. Muslim, R.A. Kadhim, M.M. Kadhim and M. Zaid, Optical properties of different organic compounds : experimental and theoretical studies, *Int. J. Pharm. Res*., 2020, **12**, 798–806.
22. A.H. Radhi, E.AB. Du, F.A. Khazaal, Z.M. Abbas, O.H. Aljelawi, S.D. Hamadan, H.A. Almashhadani and M.M. Kadhim, HOMO-LUMO Energies and Geometrical Structures Effect on Corrosion Inhibition for Organic Compounds Predict by DFT and PM3 Methods, NeuroQuantology, 2020, **18**, no. 1, 37–45. doi: 10.14704/nq.2020.18.1.NQ20105
23. D. Hussain, A. Rheima, S. Jaber and M. Kadhim, Cadmium Ions Pollution Treatments in Aqueous Solution Using Electrochemically Synthesized Gamma Aluminum Oxide Nanoparticles with DFT study, *Egypt. J. Chem*., 2019, **63**, no. 2, 417–424.
24. E.A. Yaqo, R.A. Anaee, M.H. Abdulmajeed, I.H.R. Tomi and M.M. Kadhim, Aminotriazole Derivative as Anti-Corrosion Material for Iraqi Kerosene Tanks: Electrochemical, Computational and the Surface Study, *ChemistrySelect*, 2019, **4**, no. 34, 9883–9892. doi: 10.1002/slct.201902398
25. R.A. Anaee, I.H.R. Tomi, M.H. Abdulmajeed, S.A. Naser and M.M. Kathem, Expired Etoricoxib as a corrosion inhibitor for steel in acidic solution, *J. Mol. Liq*., 2019, **279**, 594–602.

26. E.A. Hussein, D.Y. Fanfoon, R.A.H. Al-uqaily, A.M. Salman, M.M. Kadhim, A.W. Salman and Z.M. Abbas, *Mater. Today: Proc*., 1-Isoquinolinyl phenyl ketone as a corrosion inhibitor: A theoretical study, *Mater. Today Proc*., 2021, **42**, no. 5, 2241–2246. doi: 10.1016/j.matpr.2020.12.310
27. M.Z. Ghdhayeba, K.J. Sabaha, A.W. Salmanb and M.M. Kadhim, New Ag(I) and Pd(II) complexes derived from symmetrical and asymmetrical NHC precursors: Synthesis, Characterization, Antibacterial activity, and Theoretical calculations, *J. Mol. Struct*., 2021, **1245**, no. 5, 131254.
28. D.R. Koes, M.P. Baumgartner and C.J. Camacho, Lessons learned in empirical scoring with smina from the CSAR 2011 benchmarking exercise, *J. Chem. Inf. Model*., 2013, **53**, 1893–1904.
29. Æ. Frisch, R.E. Plata and D.A. Singleton, Gaussian 09W Reference, *J. Am. Chem. Soc*., 2009, **137**, 3811–3826. doi: 10.1021/ja5111392
30. H. Li, K.S. Leung, P.J. Ballester and M.H. Wong, Istar: A web platform for large-scale protein-ligand docking, *PLoS One*, 2014, **9**, e85678.
31. A.O. Zacharias, A. Varghese, K.B. Akshaya, M.S. Savitha and L. George, DFT, spectroscopic studies, NBO, NLO and Fukui functional analysis of 1-(1-(2,4-difluorophenyl)-2-(1H-1,2,4-triazol-1-yl)ethylidene) thiosemicarbazide, *J. Mol. Struct*., 2018, **1158**, 1–13. doi: 10.1016/j.molstruc.2018.01.002
32. J. Ignacio, Why is the dual descriptor a more accurate local reactivity descriptor than Fukui function? *J. Math. Chem*., 2014, **53**, 451–465.
33. H. Wang, L. Ju, H. Castaneda, G. Cheng and B.Z. Newby, Corrosion of carbon steel C1010 in the presence of iron oxidizing bacteria Acidithiobacillus ferrooxidans, *Corros. Sci*., 2014, **89**, 250–257.
34. A.A. Khadom, M.M. Kadhim, R.A. Anaee, H.B. Mahood, M.S. Mahdi and A.W. Salman, Theoretical evaluation of Citrus Aurantium leaf extract as green inhibitor for chemical and biological corrosion of mild steel in acidic solution: Statistical, molecular dynamics, docking, and quantum mechanics study, *J. Mol. Liq*., 2021, 116978.
35. M.M. Kadhim, A.W. Salman, A.M. Zarzoor and W.R. Kadhum, Inhibition of SARS-CoV-2 reproduction using Boswellia carterii: A theoretical study, *J. Mol. Liq*., 2021, **337**, 116440. 10.1016/j.molliq.2021.116440
36. A.S.M. Al-Janabi, M.M. Kadhim, A.I.A. Al-Nassiry and T.A. Yousef, Antimicrobial, computational, and molecular docking studies of Zn(II) and Pd(II) complexes derived from piperidine dithiocarbamate, *Appl. Organomet. Chem*., 2020, 1–15. doi: https://doi.org/10.1002/aoc.6108
37. T.M. Sridhar, U.K. Mudali and M. Subbaiyan, Preparation and characterisation of electrophoretically deposited hydroxyapatite coatings on type 316L stainless steel, Corros. Sci., 2003, **45**, 237–252.
38. H.A. Al-Mashhadani *et al*., Anti-Corrosive Substance as Green Inhibitor for Carbon Steel in Saline and Acidic Media, in *J. Phys.: Conference Series*, 2021, vol. 1818, no. 1, IOP Publishing, p. 012128.

39. H. Almashhadani and K. Alsaadie, Corrosion Protection of Carbon Steel in seawater by alumina nanoparticles with poly (acrylic acid) as charging agent, *Moroccan J. Chem*., 2018, **6**, no. 3, 455–465.
40. H.A. AlMashhadani, Corrosion Protection of Pure Titanium Implant in Artificial Saliva by Electro-Polymerization of Poly Eugenol, *Egyptian J. Chem*., 2020, **63**, no. 8, 2–3.
41. G. Khan, K.M.S. Newaz, W.J. Basirun, H.B.M. Ali, F.L. Faraj and G.M. Khan, Application of natural product extracts as green corrosion inhibitors for metals and alloys in acid pickling processes - a review, *Int. J. Electrochem. Sci*., 2015, **10**, no. 8, 6120–6134.
42. H.A. AlMashhadani and K.A. Saleh, Electro-polymerization of poly Eugenol on Ti and Ti alloy dental implant treatment by micro arc oxidation using as Anti-corrosion and Anti-microbial, *Res. J. Pharm. Technol*., 2020, **13**, no. 10, 4687–4696.

♦ ♦ ♦